

Final progress report on project entitled
**“Investigation of magnetoviscous and magneto-
optic properties of novel ferrofluids”**

(2010-2013)

Sponsoring Agency: University Grants Commission, New Delhi

UGC Reference No.F:37-367/2009(SR)

Principal Investigator

Dr. D. Mohanta

Department of Physics

Tezpur University

P.O. Napaam, Tezpur-784028

Assam, India

REPORT

Through this project two major kinds of ferrofluids (FFs) namely, iron oxide (Fe_3O_4 , magnetite) and gadolinium oxide (Gd_2O_3) FFs have been investigated. Magnetite is the most commonly used magnetic system known for its high saturation magnetization, easy synthesis procedure and fairly low toxicity. On the other hand, Gd_2O_3 being a stable rare earth oxide system, is capable of exhibiting unusual luminescence and magneto-optic features when doped with other dopants (e.g. europium). Unlike iron based systems, rare earth oxide based FFs have not yet received much attention owing to difficulty in preparing nanoparticles through top-down approach. Being thermally and chemically stable they need special synthesis protocol. Both iron and RE oxide based FFs were found to exhibit improved magneto-optic responses e.g., effective linear dichroism and Faraday rotation (FR). Moreover, rheological and magneto-viscous characteristics of the FFs have been explored in ambient environment. The effect of surfactant, rare earth doping, and gamma (γ) irradiations have also been considered while investigating synthesized FFs. Research outcome is being elaborated along with synthesis protocols, experimental techniques and important findings.

1. Experimental: materials and methods

(a) The preparation of a stable water-based FF required coating of the magnetic nanoparticles (MNPs) with a layer of surfactants. First, we synthesized magnetite (Fe_3O_4) particles by a co-precipitation method following an earlier method with some modification [1]. At constant stirring (~ 200 rpm), FeCl_3 and FeCl_2 (in the molar ratio $\text{Fe}^{+2}/\text{Fe}^{+3} = 0.5$) were transferred simultaneously to a conical flask containing 25 ml of 0.4 N HCl. Then, 200 μl of oleic acid ($\text{C}_{18}\text{H}_{34}\text{O}_2$, 99% pure, Otto) was mixed with 3 ml of AR-grade acetone and then transferred to the above precursor. The resulting solution was added drop-wise to 250 ml of 1.5 M NaOH solution under vigorous stirring. To facilitate the reaction, 100 μl of oleic acid was added in steps, in 10 min interval. This has resulted in a dark black colouration. In the precursor, the nanoparticle growth was allowed to proceed for 30 min at 30°C and under constant stirring. Finally, it was allowed to cool down to room temperature and by performing repeated washing, centrifugation and decantation, we obtained the product of surfactant-coated magnetite particles.

2. Results and discussion

2.1 X-ray diffraction (XRD) analysis

The synthesized MNPs were first characterized by XRD. Figure 1(a) is a typical XRD pattern of the synthesized product, which is characterized by five distinct peaks located at 29.87° , 35.15° , 42.92° , 56.84° and 62.4° and corresponding to (220), (311), (400), (511) and (440) planes of inverse spinel crystal structure of magnetite system. In order to estimate average crystallite size (d), we used the Williamson–Hall (W-H) equation given by [2]:

$$\beta_{hkl} \cos \theta_{hkl} = 0.9\lambda/d + 4\eta \sin \theta_{hkl}$$

The W-H plot was drawn considering prominent XRD peaks (Fig. 1(b)). In our system, the microstrain and average crystallite size are estimated to be -7×10^{-2} , and ~ 7 nm; respectively.

The XRD pattern of the synthesized Gd_2O_3 nanopowder is shown in Fig. 1(c) which is characterized by five prominent peaks located at respective Bragg angles (2θ) of 28.52° , 33.10° , 43.54° , 47.19° , and 56.19° . These peaks corresponded to (222), (400), (431), (440), and (622) planes of C-type cubic phase (with space group, $Ia\bar{3}$) with preferred crystallographic orientation along (222) plane (JCPDS 36-1451). Even with mild amount of Tb^{3+} ion doping, the peak positions were found to remain intact. This signifies incorporation of the impurity ions into the host Gd_2O_3 and that, the existence of other byproducts/phases is fairly unlikely.

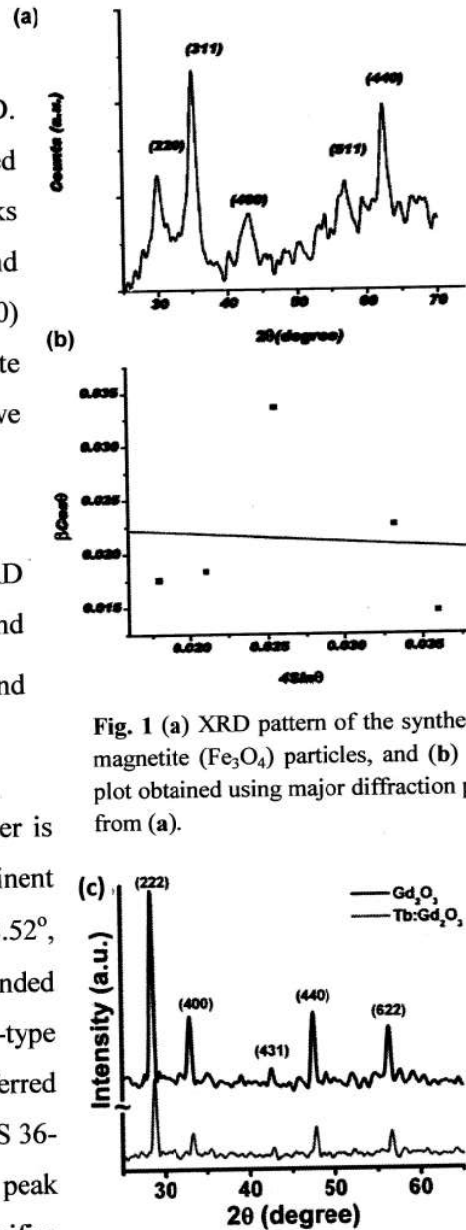


Fig. 1 (a) XRD pattern of the synthesized magnetite (Fe_3O_4) particles, and (b) W-H plot obtained using major diffraction peaks from (a).

Fig.1(c): XRD patterns of the synthesized nanopowders: undoped and Tb^{3+} doped Gd_2O_3 nanopowders.

In order to prepare a water-based FF, ~2 g of oleic acid coated MNPs were added to 40 ml of milli-Q water and then heated to 60°C under vigorous stirring, for 1 h. Simultaneously, a separate solution of oleic acid, milli-Q water and a few drops of NH₄OH was prepared and added to it to get a stable solution (pH = 10.2). The as-prepared FFs were irradiated with γ - photons available from a γ -source (⁶⁰Co chamber) that is capable of emitting photons with an average energy of ~1.25 MeV and at a dose rate of 1.8 Gy/sec. For making a comparative analysis with reference to the pristine FF sample, we considered two γ - doses, of 878 Gy and 2.635 kGy.

(b) In order to prepare nano-sized Gd₂O₃ powders, we have followed a low-cost physico-chemical route. In this method, bulk Gd₂O₃ was first converted into a nitrate compound. Then, a subsequent reduction has led to the hydroxide and oxide products. At first, 1 mmol of bulk Gd₂O₃ (99%, Otto) was added to 50 ml of double-distilled water. Next, an appropriate amount of HNO₃ (69%GR, Merck) was transferred to this solution under vigorous stirring until a clear solution of Gd(NO₃)₃ is obtained. The solution was diluted to 100 ml in a volumetric conical flask by adding more amount of distilled water. Subsequently, 3.3 g of N-cetyl-N,N,N-trimethylammonium bromide (CTAB) was added at 65°C, which resulted in a yellow coloured precursor. 10 ml of freshly prepared 0.006 M aqueous NaOH was transferred to the sol after it was cooled down to the room temperature. As a result, a white precipitate of Gd(OH)₃ was formed which was then subjected to vigorous stirring (30 min), and centrifugation (30 min). In order to obtain the finest quality precipitate, the as-received product was subjected to repeated washing with warm distilled water and centrifugation. The precipitate was dried in air and heated at 800°C for 1 h, till an off-white powder of Gd₂O₃ is received. In order to prepare a stable FF system, surfactant-coated particles were required to get dispersed in a carrier fluid. We opted ethanol as our carrier medium since CTAB is chemically inert in ethanol. The CTAB-coated Gd₂O₃ nanoscale powder was dissolved in ethanol followed by stirring overnight. The as-prepared FF was then divided into six equal parts for carrying out irradiation experiment independently. The as-prepared FF was irradiated with a γ -photons obtained from a source γ -source (⁶⁰Co chamber) that is capable of emitting photons with an average energy of 1.25 MeV at a dose rate of 1.8 Gy/s. Keeping in mind the amount of doses used by earlier workers, we have selected five doses (e.g., 32, 97, 292, 878 Gy and 2.635 kGy) in this case.

2.2 Transmission electron microscopic (TEM) analysis

The direct proof of evidence on the formation of nanoparticles can be assessed from TEM studies. Figure 2 depicts TEM images of ultrasonically agitated magnetite particles of pristine and γ -irradiated Fe_3O_4 MNP-based FFs. It is evident that the particles retain their spherical shape both in case of the pristine FF and the one which was irradiated with a dose of 878 Gy (Fig. 2(b)) except the fact that, the particles existed in unclustered form in the later case. When the FF was irradiated with a comparatively higher dose (2.635 kGy), some noticeable structural changes were observed. In the pristine FF, the particles were of average size ~ 8 nm. As can be found from the micrographs, the γ -irradiated FFs were likely to contain a substantial amount of larger particles along with smaller ones. The MNPs, with an average size of ~ 20 , and 48 nm were observed in case of the FFs irradiated with a dose of 878, and 2.635 kGy; respectively.

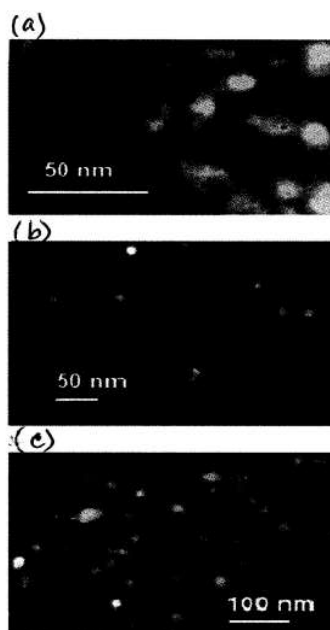


Fig. 2: TEM micrograph of (a) pristine and γ -irradiated nanoparticles present in the FFs treated with a dose of (b) 878 Gy, (c) 2.635 kGy.

The average size of the Gd_2O_3 nanoparticles, as revealed from the below micrograph, is ~ 9 nm. The particles are found to be nearly spherical, with a distinct lattice fringe pattern and an interplanar spacing of ~ 0.28 nm (Fig. 3(a)). The predicted value of the interplanar spacing corresponds to the separation of (0 0 3) planes of the monoclinic Gd_2O_3 structure. Figure 3(b) represents the HRTEM image of the irradiated (dose: 2.635 kGy) sample.

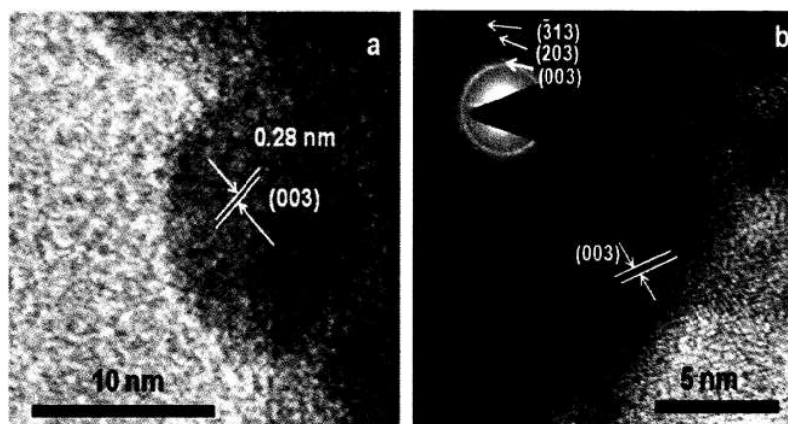


Fig. 3: HRTEM image of (a) pristine and (b) γ -irradiated Gd_2O_3 nano-particles (dose: 2.635 kGy). Inset of (b) is the SAED image.

The inset of Fig. 3(b) depicts the selected area electron diffraction (SAED) pattern of the irradiated specimen. The diffused but distinguishable rings were indexed as (003), (203), and ($\bar{3}$ 13) which confirm with the XRD patterns of the monoclinic Gd₂O₃ phase.

Fig. 4(a) and upper inset depicts low and high resolution TEM micrograph of the synthesized C-type Gd₂O₃ nanopowder sample. The distinct and well resolved lattice fringes can be seen from the image along with an interplanar spacing of \sim 0.311 nm, among consecutive (222) planes (upper inset of Fig. 4(a)). The HRTEM image of the γ irradiated Gd₂O₃ nanoparticles and irradiated with a dose rate of 2.635 kGy is shown in Fig. 4(b).

The HRTEM images of both un-irradiated and irradiated Tb doped Gd₂O₃ samples are presented in Figs. 4(c) and (d), respectively. Fig. 4(c) shows an isolated, unexposed spherical particle of size \sim 7 nm, which depicts distinct, equispaced crystal lattice planes (shown by short parallel lines) and having an interplanar spacing of \sim 0.311 nm corresponding to successive (222) planes of the cubic Gd₂O₃ (Fig. 4(c)).

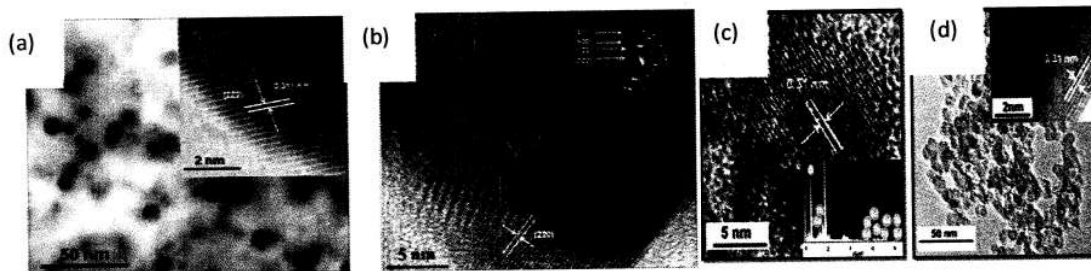


Fig. 4: TEM image of the (a) un-irradiated Gd₂O₃ powder sample with lattice fringe of an isolated particle shown as the figure-inset. (b) HRTEM image of the synthesized Gd₂O₃ nanopowder irradiated with the γ -rays at a dose of 2.635 kGy. The upper inset is the corresponding SAED pattern. HRTEM images of (c) un-irradiated and (d) irradiated (dose: 2.635 kGy) Tb³⁺ doped Gd₂O₃ nanoparticles. An EDX spectrum of the un-irradiated system is shown as inset in (c). A distributed view of the nanoparticles and interplanar spacing of (222) plane of the irradiated nanosystem are depicted in (d).

2.3 Dynamic light scattering (DLS) studies

Figure 5(a) is the size distribution of the un-irradiated Fe₃O₄ FF which predicts that the most of the particles are having an average size of \sim 15 nm. In case of the Fe₃O₄ FF irradiated with a dose of 878 Gy, the average particle size has been increased to \sim 28 nm and the specimen subjected to a comparatively higher dose (2.635 kGy), it is predicted as \sim 60 nm. Thus, adequate particle growth, as a result of γ -radiation, is quite evident from the DLS studies.

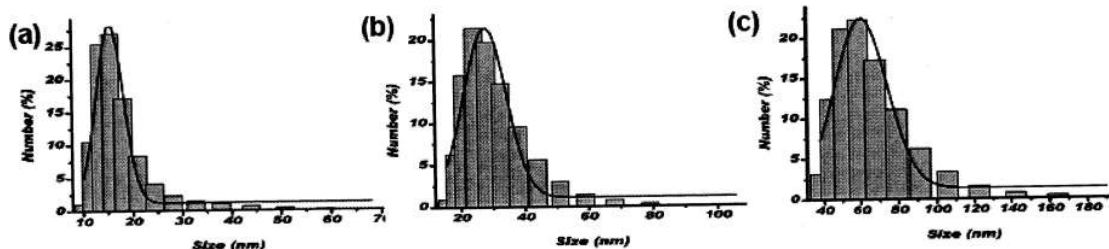


Fig. 5 DLS study of the (a) pristine and γ -irradiated magnetite based ferrofluid with doses (b) 878 Gy and (c) 2.635 kGy

In order to know the particle size distribution under hydrodynamic interactions, the unexposed and irradiated Gd_2O_3 based FFs were also analyzed through DLS studies. Fig. 6(a) depicts the size distribution of the un-irradiated FF, which predicts that most of the particles are having an average diameter of ~ 7.9 nm and full width at half maxima (FWHM) of ~ 4.4 nm. In case of the FF irradiated with a dose of 2.635 kGy, the average size is approximately ~ 8 nm and with a FWHM ~ 3.3 nm (Fig. 6(b)).

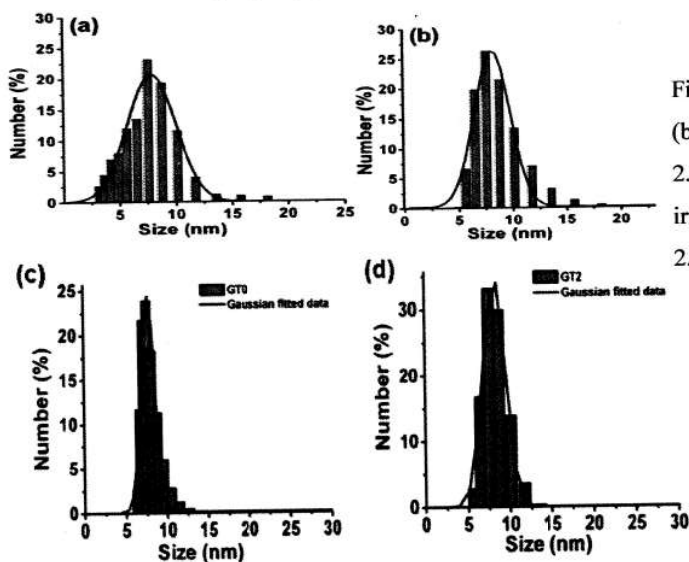


Fig.6. DLS study of the (a) un-irradiated and (b) γ -irradiated Gd_2O_3 based FF at a dose of 2.635 kGy. (c) un-irradiated and (d) γ -irradiated $Tb:Gd_2O_3$ based FF at a dose of 2.635 kGy

Fig. 6(c) shows the DLS spectra of the un-irradiated $Tb:Gd_2O_3$ based FF which predicts that most of the particles have a normal size distribution and with a typical average size of ~ 8 nm. In case of the FF irradiated with a dose of 2.635 kGy, the average size was ~ 8.5 nm (Fig. 6(d)).

2.4. Fourier transform infrared (FT-IR) spectroscopy studies

Figure 7 shows the room temperature FT-IR spectra of the pristine and the irradiated Fe_3O_4 FFs. Except a peak observable at $\sim 2077\text{ cm}^{-1}$ and identified as C–O stretching mode of the atmospheric CO_2 molecule, all other peaks correspond to the chemical constituents available in the FF under study. The broad band at $\sim 3488.07\text{ cm}^{-1}$ and the small peak at $\sim 2403\text{ cm}^{-1}$ represent the characteristic O–H bending and stretching vibrational modes of hydroxyl group of the water molecule. The sharp peak at $\sim 1670\text{ cm}^{-1}$ and a weak peak at $\sim 1161\text{ cm}^{-1}$ witness the signatures of strong and medium –CO–OH bonding of the oleic acid. The typical Fe–O stretching vibration of Fe_3O_4 is prominent in the lower wavenumber regions, in the range $598\text{--}566\text{ cm}^{-1}$ and $510\text{--}445\text{ cm}^{-1}$. It is seen that, upon irradiation, the characteristic peak of Fe_3O_4 is down-shifted toward a lower wavenumber side.

Figure 8 depicts the FT-IR spectra of the γ -irradiated Gd_2O_3 nanoparticle based (monoclinic phase) FFs. The conventional peaks appearing at ~ 3403 and 2400 cm^{-1} represent the respective signatures of O–H stretching and C–O stretching of atmospheric water and CO_2 molecules. In ethanol medium, bending modes of CH_3 and CH_2 are observable at ~ 1392 and 1452 cm^{-1} , respectively; whereas CH_2 , CH_3 , CO and OH stretching vibrations were observable at ~ 2910 , 2975 , 1060 and 3679 cm^{-1} [3]. The weak band at 2980 cm^{-1} and the sharp band at 1550 cm^{-1} have arisen due to CTAB (–CH) in the samples [4].

Different peaks that are assigned to various components of Gd_2O_3 based FFs are listed in Table 1. It is quite evident that, the vibrational features corresponding to the Gd–O bonds have been significantly influenced by the irradiation effect. A close look on the spectra has revealed that, the peak becomes more prominent with increasing γ -dose. But an anomaly in the Gd–O

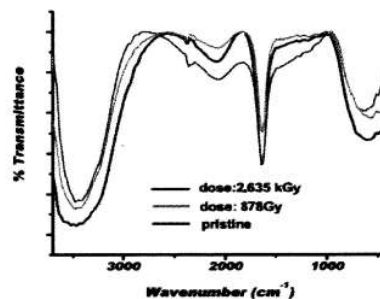


Fig. 7: FT-IR spectra of pristine and irradiated Fe_3O_4 FFs

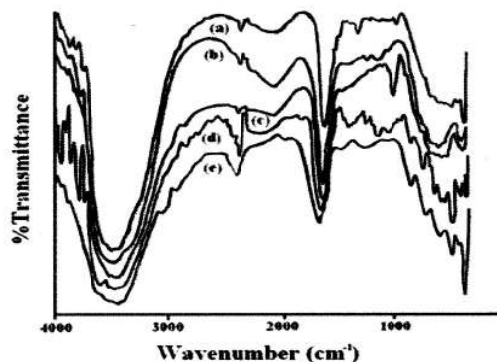


Fig. 8. FT-IR spectra of the FFs irradiated with different γ -doses: (a) 32 Gy, (b) 97 Gy, (c) 292 Gy (d) 878 Gy and (e) 2.635 kGy

vibration mode with discontinuities and less intensity profile was observed in case of the FF irradiated with a dose of 878 Gy. Note that, defects like oxygen vacancies are very common in oxide compounds. Some Gd vacancies produced during synthesis may also exist in the system. Additionally, the creation of a large number of free electrons by the energetic γ -rays (1.25 MeV) can be responsible for adequate defect manifestation in Gd_2O_3 system.

Figure 9 represents the FT-IR spectra of the GT0, GT1, and GT2 samples. Except the broad peaks located at ~ 3500 and 2400 cm^{-1} and corresponding to the O-H and C-O stretching modes of the atmospheric water and CO_2 , all others peaks represent characteristic features of the nanoparticles and the carrier fluid (comprising organic molecules). The CH_3 and CH_2 bending modes of ethanol were observable at ~ 1392 and 1452 cm^{-1} , whereas CH_2 , CH_3 , CO, and OH stretching vibrations were found to be located at ~ 2910 , 2975 , 1060 , and 3679 cm^{-1} ; respectively. In the present case, we assign the band ~ 1384 – 1392 and 1452 – 1469 cm^{-1} to symmetric CH_3 and CH_2 vibrations. In order to understand the vibrational features of the inorganic Gd_2O_3 nanoparticles in the carrier fluid (organic media), we need to focus our attention to the lower inset of Fig. 9. The bands at ~ 558 and 445 cm^{-1} were believed to be caused by the stretching vibrations of Gd–O, due to Gd_2O_3 system itself. For GT1 and GT2 systems, the characteristic peak was found to shift toward a lower wavenumber value, of ~ 550 and 540 cm^{-1} ; respectively.

Table 1. Assigned modes in the FT-IR spectra.

| Peak position (cm^{-1}) | Assigned mode |
|------------------------------------|--|
| 2980 | C- CH_3 asymmetric stretching and N- CH_3 symmetric stretching of CTAB |
| 1550 | $-CH_2-$ and $-CH_3$ stretching of CTAB |
| 1384–1392 | CH_3 vibration of ethanol |
| 1452–1469 | CH_2 vibration of ethanol |
| 1058 | C-O vibration of ethanol |
| 536 | In-plane Gd-O vibration |

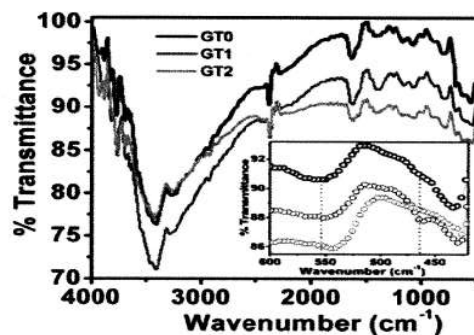


Fig. 9. FT-IR spectra of GT0, GT1, and GT2 FFs exhibiting different stretching and bending vibrations.

2.5 UV-visible optical absorption spectroscopy studies

The UV-visible optical absorption spectra of the un-irradiated (GT0) and irradiated (GT1: 92 Gy; GT2: 2.635 kGy) FFs are shown in Figure 10. Basically, a sharp absorption peak, which corresponds to $^8S_{7/2} - ^6I_{7/2}$ transition of Gd^{3+} ions is the characteristic feature of all the Gd_2O_3

nanoparticle systems. As demonstrated schematically in Figure. 11, with increasing γ -dose, the Compton events were on the rise and consequently, creation of defects becomes more prominent.

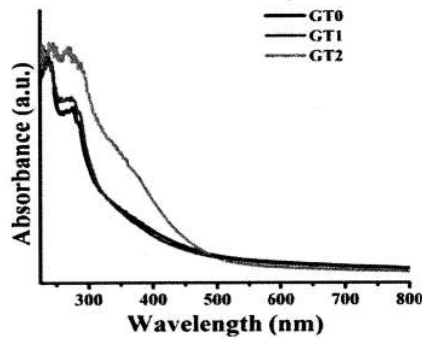


Fig. 10: UV-Visible optical absorption spectra of GT0, GT1, and GT2 FFs

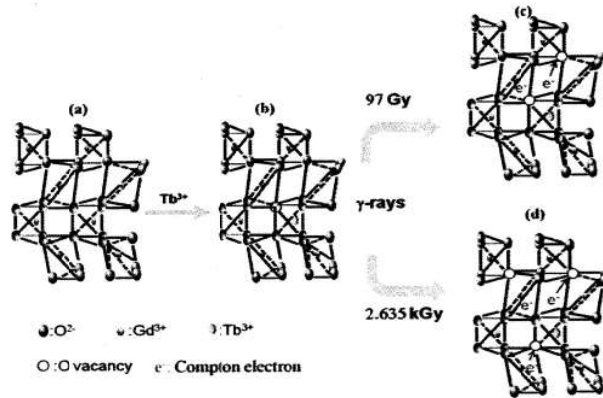


Fig. 11: Schematic illustration of dopant and irradiation induced changes in the lattice structure of (a) C-type Gd_2O_3 lattice, (b) modified lattice due to incorporation of Tb^{3+} ions. The production of Compton electrons along with the generation of oxygen vacancies at a γ -dose of 97 Gy and 2.635 kGy are highlighted in (c) and (d), respectively

2.6. Photoluminescence studies

The room temperature PL spectra ($\lambda_{ex} = 270$ nm) of un-irradiated and irradiated FFs are shown in Figure 12(A). The un-irradiated FF has experienced an asymmetrically broadened spectrum peaking at ~ 355 nm. Earlier reports have suggested that, this peak can be attributed to ${}^6P_{7/2} - {}^8S_{7/2}$ transitions of Gd(III) [5]. Also the observed asymmetry in the PL response (pristine sample) is assigned to the existence of surface defects on the nanoscale Gd_2O_3 crystallites. Upon γ -irradiation, the above-mentioned peak is red-shifted to 390 nm (where band-to-band emission can be superimposed with the defect emission). In this system, besides the already existing point defects (vacancies), plentiful other meta-stable, surface defects are created due to impact of γ -irradiation. In order to correlate the amount of defect formation, asymmetry introduced and -dose, we have performed deconvolution mechanism on each of the PL spectra (Figure 12B).

For the sake of clarity and better understanding, we have estimated symmetry factor (S) and correlated with the intensities of the deconvoluted peaks with respect to the original peak. Note that right symmetry (S_R) is related to the defect emission process whereas left symmetry (S_L) is associated with the band-to-band emission. Figure 13(a) represents the variation of relative right

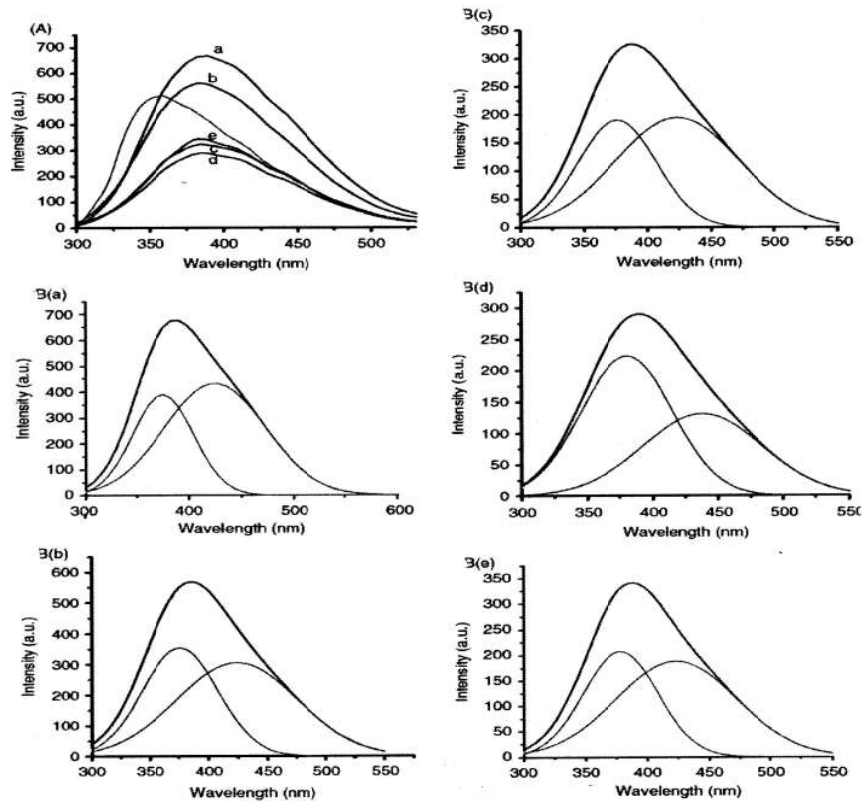


Fig 12. Room temperature PL response of (A) unirradiated and γ -irradiated Gd_2O_3 FFs with doses (a) 32 Gy, (b) 97 Gy, (c) 292 Gy, (d) 878 Gy and (e) 2.635 kGy. (B) (a)–(e) representing respective deconvolution of individual PL peaks of the irradiated samples.

symmetry factor as well as relative intensity (I_2/I_1 , I_2 being the intensity of the defect emission after deconvolution and I_1 is the intensity of the main peak) obtained from the deconvolution. Figure 13(b) with relative intensity as I_1/I_2 (I_1 is the intensity of the deconvoluted band-to-band emission) and relative symmetry factor S_L/S (S_L is the left symmetry factor of the pristine sample). The non-linear nature of the curve indicates the simultaneous effect of defect formation/passivation in the irradiated system. Firstly, with the increasing dose from 32 to 97

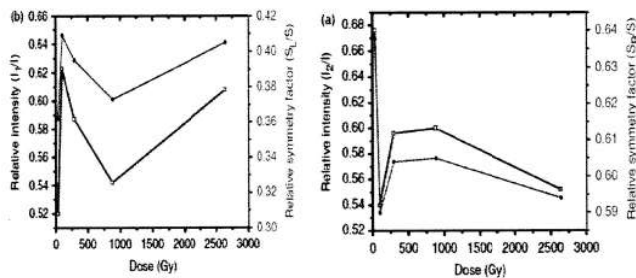


Fig. 13. Variation of relative intensity and relative symmetry factor vs. dose corresponding to (a) defect-related emission and (b) band-to-band emission.

Gy, we observed a drastic reduction in the relative PL intensity which may be ascribed to adequate passivation of surface defects. A further increase in dose to 292 and 878 Gy is characterized by significant enhancement of I_2/I ratio. At the highest dose (2.635 kGy), we noticed a reduction of I_2/I value. The relative symmetry factor (S_R/S) also gives a similar pattern. The room temperature PL spectra ($\lambda_{ex}=270$ nm) of un-irradiated (G0) and irradiated (G1:92 Gy; G2: 2.635 kGy) FFs are shown in Fig. 14(a). In order to make out a clear picture of the PL peaks, we have introduced Gaussian fitting to each of the spectra, for pristine and irradiated samples (Fig. 14(b) (i) G0, (ii) G1 and (iii) G2) separately. The peak position at ~ 313 nm corresponds to intra $4f$ carrier transition ($^8S_{7/2} \rightarrow ^6P_{7/2}$) associated with the Gd^{3+} ions. The peak maxima at ~ 350 nm is due to the defect related emission, originated via oxygen vacancies (V_O). The deep UV

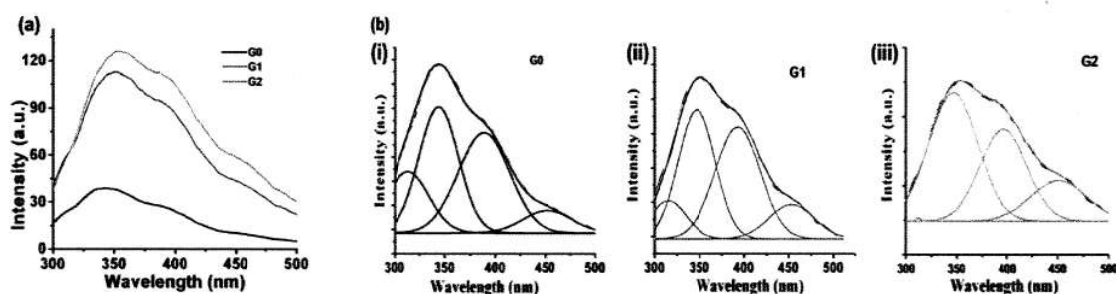


Fig. 14a. Room temperature PL spectra of G0, G1 and G2 FFs (b). Individual Gaussian fitted spectra for (i) G0, (ii) G1 and (iii) G2 FFs.

blue band located at ~ 400 nm is attributed to the recombination of a delocalized electron close to the conduction band with a single charged state of surface oxygen vacancy and in accordance with Wang's proposition [6]. The blue emission at ~ 450 nm is attributed to radiative responses mediated through surface defects of both Schottky and Frenkel types [7].

The room temperature PL emission spectra of the GT0, GT1, and GT2 FFs, excited at a wavelength of 300 nm, are presented in Fig. 15(a). In order to obtain a clear idea about the peak positions, we have introduced the normalized Gaussian fitting on each of the experimental curves, and the results are presented in Figs. 15(b)–15(d). The band at ~ 430 nm was believed to be originated from the defect states of Frenkel or Schottky types. Upon γ -irradiation, the above mentioned peak is red-shifted to ~ 445 nm. The emission peaks positioned at ~ 490 and 540 nm were ascribed to $^5D_4-^7F_6$ and $^5D_4-^7F_5$ transitions of Tb^{3+} ions [8]. Finally, a representative PL excitation spectrum corresponding to an emission wavelength of ~ 540 nm is shown in Fig. 15(e).

The excitation peak at ~254 nm corresponds to the inter ionic energy transfer due to effective matching of the excited states ($4f$ levels) of Gd^{3+} and Tb^{3+} ions. Moreover, the peak at ~285 nm and those between ~345 and 400 nm are believed to be originated from the $4f$ intra configuration of Tb^{3+} ions, as predicted in earlier works [9].

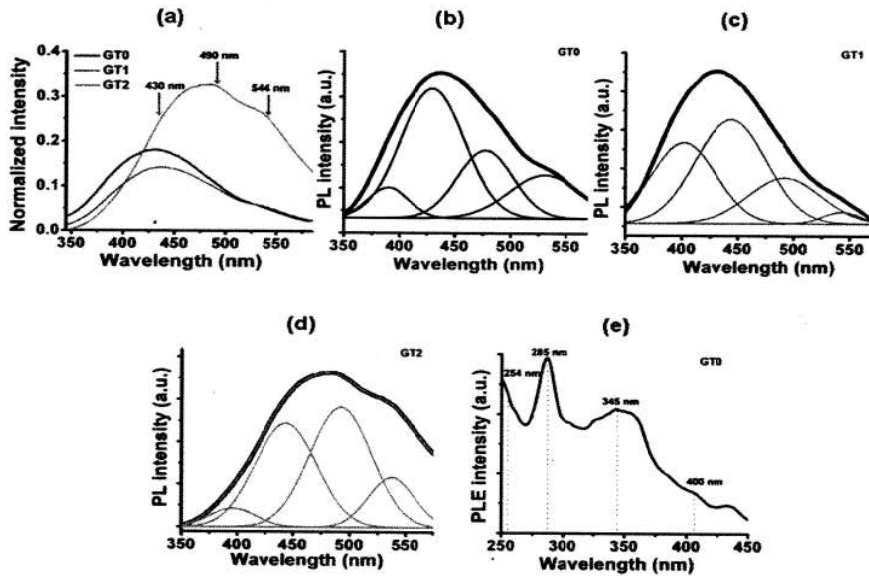


Fig. 15 (a) Room temperature PL spectra of GT0, GT1, and GT2 FFs excited at a wavelength of 300 nm. The Gaussian fitted spectra are shown separately in (b) GT0, (c) GT1, and (d) GT2. A PL excitation spectrum (at emission ~540 nm) for GT0 is shown in (e).

2.7 Magneto-optic Faraday effect

When optical activity of a material under study changes with the application of a magnetic field, the corresponding effect is called as magneto-optic effect. Magneto-optic effect is important in the sense that it provides information regarding the electronic and the spin structure of the system. The orientation of the light polarization in a medium can be studied either in the transmission mode (Faraday rotation, FR) or in the reflection mode (Kerr effect). FR is the measure of the interaction of a plane polarized light with matter in presence of an external magnetic field applied along the direction of light wave propagation. When a polarized light beam is transmitted through an optically active matter, it undergoes transformation into two circularly polarized light beams. Generally [10], FR (θ_F) is expressed as $\theta_F = VHI$, where V is the Verdet constant of the material, H is the applied magnetic field and I is the optical path length. A

custom-made FR set-up is shown schematically in Fig. 16a. In order to calibrate our set-up using a wavelength of 632.8 nm, first we measured the FR of milli-Q water taken in a 1 cm cuvette with empty cuvette as reference (Fig. 16b). The FR responses of the pristine FF (Fe_3O_4 -based) measured for two different wavelengths (532 and 632 nm) are shown in Fig. 16c. For a given wavelength, the FR gradually increases with the applied field, and then exhibits a saturation trend. Considering chaining effect into account the FR of FFs can be expressed as $\theta_F = CM/(H)M_S + VHI(H)$. It was also revealed that, at a definite magnetic field, the FR is dependent on the excited wavelength (Fig. 16c). The Faraday responses of the irradiated and pristine FFs (working wavelength 632 nm) are shown in Fig. 16d. The FR was found to be improved with the irradiation dose.

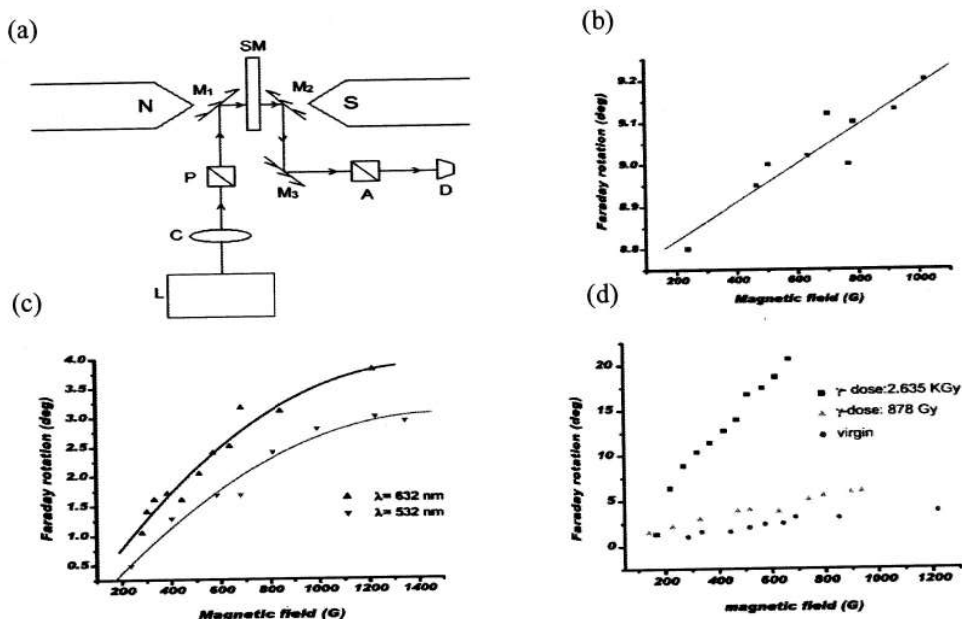


Fig. 16a Schematic experimental set-up for Faraday rotation measurement with *L*: laser, *C*: collimator (lens), *P*: polarizer, *SM*: specimen, (*M1*, *M2*, *M3*): mirror, *A*: analyser, *D*: photodetector. b) Faraday rotation of milli-Q water c) Faraday rotation response of un-irradiated FF at two different wavelengths and d) Faraday rotation response of pristine and irradiated FFs.

Quantitatively, the Verdet constant, as calculated from the linear part, was found to improve from a magnitude of 0.64×10^{-2} deg/G-cm for pristine FF, to a value of 5.9×10^{-2} deg/G-cm for the FF subjected to γ irradiation (dose: 2.635 kGy). In Fe_3O_4 system, $3d$ electronic states of iron are generally responsible for the observable magneto-optic effect.

Fig 17(a) shows the FR response of pristine (G0) and γ irradiated (G1:868 Gy; G2: 2.635 kGy) samples. The figure inset depicts the FR response of specimen G0 while using 532 and 632.8 nm wavelengths of two different lasers. For γ irradiated FF samples, a substantial improvement of the FR can be found, as evident from the plots shown in Fig. 17(a). In reference to G0 and G1, the response of the specimen G2 has revealed that the saturation trend could be realized at a relatively higher magnetic field. The results of individual cases are highlighted in Fig. 16(b), and the linear fitting of each of the cases gives the manifested optical length δl (differential FR can be expressed as $\frac{d\theta}{dH} = V(l + \delta l)$ where, θ is the FR at magnetic field H , V is the Verdet constant, l is the optical path length and δl being variation in the optical length). The estimated values for G1 and G2 specimens are 0.04 and 0.132 cm, respectively.

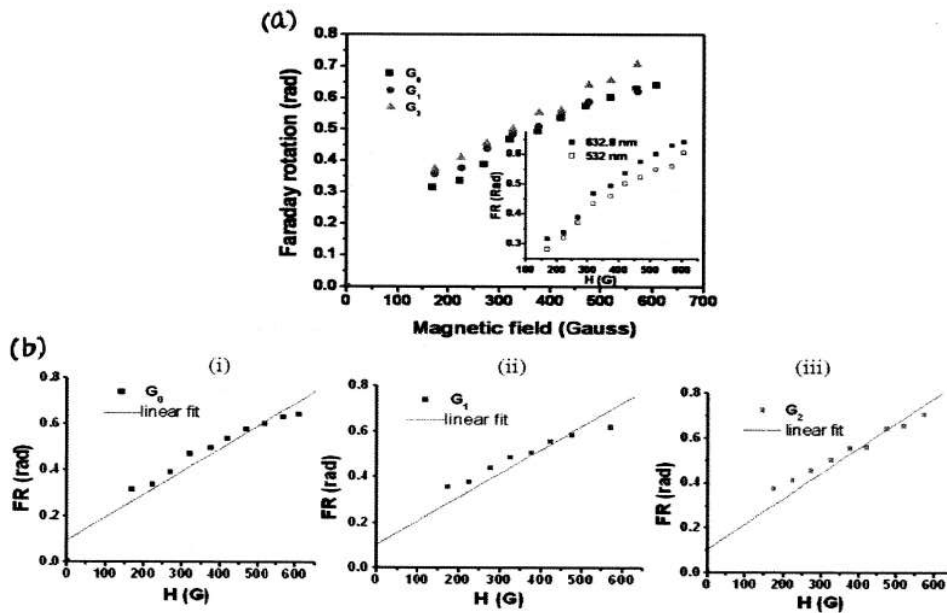


Fig. 17 (a) Field-dependent Faraday rotation for samples G0, G1, and G2 FFs using 632.8 nm laser source. Inset shows response of G0 using 532 and 632.8 nm lasers. (b) Individual cases with linear fits for (i) G0, (ii) G1, and (iii) G2 FFs.

2.8 Magneto-optic response and dichroism

The linear dichroism (LD) was measured using the same setup as used for the FR measurements, but with different configuration. Measurements were made with the plane polarized light parallel and perpendicular to the applied magnetic field and corresponding values of parallel and

perpendicular dichroism, ΔA_{\parallel} and ΔA_{\perp} , are defined as the changes in the absorbance of the sample caused by turning on the magnetic field. We write [11]

$$\Delta A_{\parallel} = \ln (I_{\parallel}/I_0), \quad 1(a)$$

$$\Delta A_{\perp} = \ln (I_{\perp}/I_0), \quad 1(b)$$

where, I_{\parallel} and I_{\perp} depict transmitted light intensities in the direction parallel and perpendicular to the magnetic field and I_0 is the intensity of the incident light when it was turned off. The dichroism is also the difference in the extinction indices k_{\perp} and k_{\parallel} . Expressing transmitted light intensity in terms of extinction indices,

$$I_{\parallel} = I_0 \alpha_{\parallel} = I_0 \exp[-(4\pi) k_{\parallel}/\lambda], \quad 2(a)$$

$$I_{\perp} = I_0 \alpha_{\perp} = I_0 \exp[-(4\pi) k_{\perp}/\lambda]. \quad 2(b)$$

The magnetic dipole moment m , of the particle makes an angle θ , with the applied external field H , and hence, the orientation energy is given by,

$$U = mH \cos \theta. \quad (3)$$

$$\Delta A_{\parallel} = -2 \Delta A_{\perp}. \quad (4)$$

Fig.18(a) represents the field-dependent LD spectra of the pristine and γ -irradiated specimens.

As RE oxides are very stable against radiation, defects have been created without any structural modification. For γ -irradiated specimen, there exist a noticeable change (about 10% for G2 than G0) in the absorbance along the parallel polarization direction as compared to its counterpart. Referring to Fig. 18(b), the differential LD response was found to be almost uniform for all the specimens.

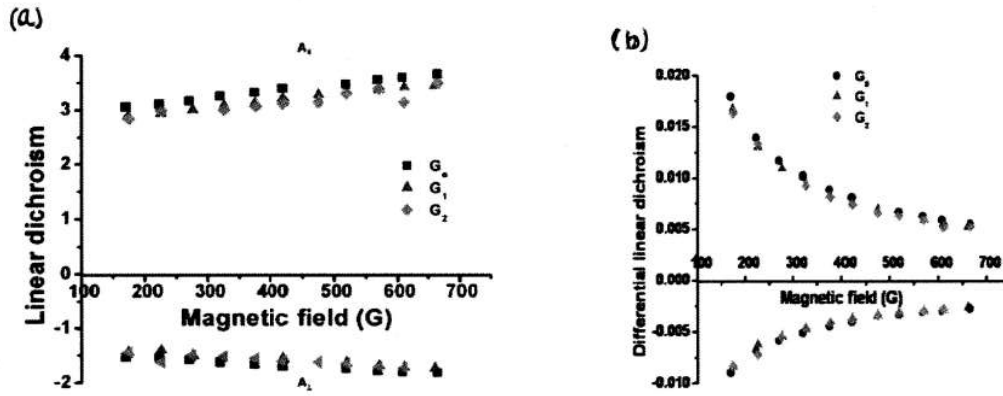


Fig. 18 (a) LD response of pristine and γ -irradiated sample using a red laser ($\lambda=632.8$ nm), and (b) the differential change of LD with the applied field.

2.9 Nonlinear viscoelastic and rheological behavior

The flow behavior (at a fixed shear stress of ~ 4.7 Pa) of the pristine and γ - irradiated Gd_2O_3 based fluids are shown in Fig. 19. All the traces show non-Newtonian characteristics with a shear thinning behavior to a variable extent. The experimental data points, obeyed bi-exponential curve fitting as given by the expression:

$$y = y_0 + A_1 e^{-(x/\tau_1)} + A_2 e^{-(x/\tau_2)} \quad (5)$$

where y_0 is the initial viscosity, y_1 and y_2 are viscosities at zero shear rate, x is the shear rate and τ_1 and τ_2 are decay parameters in sec^{-1} . From the fitted curve, it is quite evident that the viscosity of the fluid gets reduced owing to two kinds of decay phenomenon: the fast component that exhibited a higher magnitude of decay parameter and the slow component that has a lower decay component. The overall viscous nature of the FFs is characterized by a competition between the formation and break-up of the nanoparticle-based chains. From the bi-exponentially fitted curves, the fast decay parameter follows a decreasing trend with increasing irradiation dose whereas, the slow decay parameter experienced a reverse trend (Table 2). The fast decay parameter decreases from a value of $1107 sec^{-1}$ (G0) to $601.4 sec^{-1}$ for G1, and $527.8 sec^{-1}$ for G2 FF system. Also, the slow decay parameter has a decreasing trend: $23 sec^{-1}$ for G0, $21.2 sec^{-1}$ for G1, and $20 sec^{-1}$ for G2.

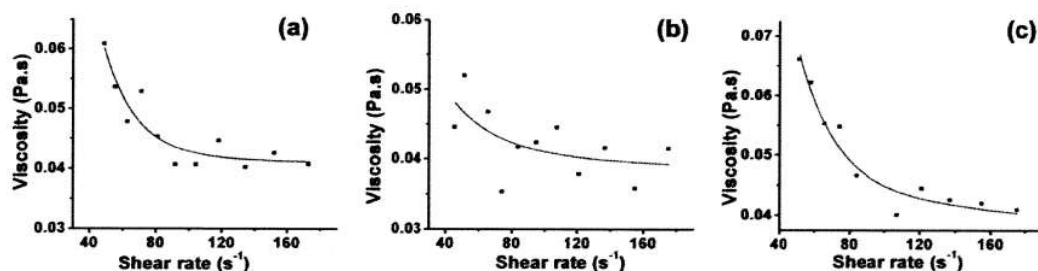


Fig. 19. Variation of viscosity with shear rate (45–175 sec⁻¹) for different FFs: (a) G0, (b) G1 and (c) G2.

Table 2
Physical parameters related to viscoelastic studies of the FFs.

| Sample | η_0 (Pa.s) | η_{45} (Pa.s) | η_{175} (Pa.s) | Decay parameter (s ⁻¹) | |
|----------------|-----------------|--------------------|---------------------|------------------------------------|----------|
| | | | | τ_1 | τ_2 |
| G ₀ | 0.075 | 0.06 | 0.047 | 1107 | 23.88 |
| G ₁ | 0.065 | 0.044 | 0.041 | 601.4 | 21.2 |
| G ₂ | 0.0807 | 0.054 | 0.040 | 527.0 | 20 |

2.10. Rheological shear thinning behavior of γ -irradiated FFs

In recent years, rheological property has emerged as an important physical property to discriminate non-Newtonian fluids from the Newtonian ones. Fig. 20(a)–(c) depicts variation of shear stress with shear rate corresponding to the un-irradiated and γ -irradiated, Tb³⁺ doped Gd₂O₃ nanoparticle based FFs. All the samples have exhibited shear thinning behavior, but to different extents and with different power indices ($\sigma = K\gamma^s$, where σ is shear stress, K is system dependent parameter and s is power index) (Table 3). For Tb-doped Gd₂O₃ nanoparticle based FF case, the s value shows an increasing trend with the irradiation dose, with respective values of 0.34, and 0.5 as for the un-irradiated specimen and the one that is irradiated with the highest dose (2.635 kGy). The shear thinning behavior i.e., variation of apparent viscosity in response to the shear rate, is shown in Figs. 21(a)–(c). As can be found, the experimental data points obey bi-exponential curve fitting, which can be expressed as: $y = y_0 + y_1 e^{-(x/\tau_1)} + y_2 e^{-(x/\tau_2)}$, where y_0 is the initial viscosity, y_1 and y_2 are viscosities at zero shear rate, x is the shear rate, τ_1 and τ_2 are decay parameters in sec⁻¹. From the bi-exponentially fitted curves (Fig. 21), the more rigid fast decay parameters as well as more flexible slow decay parameter were found to follow an increasing trend with increasing irradiation dose. The fast decay parameter (τ_1) has increased from a value of ~207 sec⁻¹ (GT0) to 1966.2 sec⁻¹ for GT1, and 2742.9 sec⁻¹ for GT2 FF specimens. Also, the slow decay parameter has experienced a rising trend with 8.6 sec⁻¹ for GT0, 16.47 sec⁻¹ for GT1, and 28.38 sec⁻¹ for GT2 systems. The fast components of GT0 and GT2 FFs have exhibited

about ~25 fold and 98 fold improvements with respect to their slow components. For the sake of comparison, we also evaluated the flow behavior of the undoped-Gd₂O₃ systems. Interestingly, a reverse trend was found for decay parameters of the un-doped system as compared to the irradiated one (Table 3).

TABLE 3. Physical parameters related to rheological studies of the FFs (with respective symbols defined in the text).

| Sample name | K | s | τ_1 (s ⁻¹) | τ_2 (s ⁻¹) |
|-------------|--------------|-------|-----------------------------|-----------------------------|
| G0 | 0.381 ± 0.13 | 0.539 | 1107 | 23.88 |
| G1 | 0.908 ± 0.08 | 0.346 | 601.4 | 21.2 |
| G2 | 0.918 ± 0.06 | 0.330 | 527 | 20 |
| GT0 | 0.947 ± 0.08 | 0.340 | 207 | 8.6 |
| GT1 | 0.551 ± 0.04 | 0.444 | 1966.2 | 16.47 |
| GT2 | 0.486 ± 0.09 | 0.500 | 2742 | 28.38 |

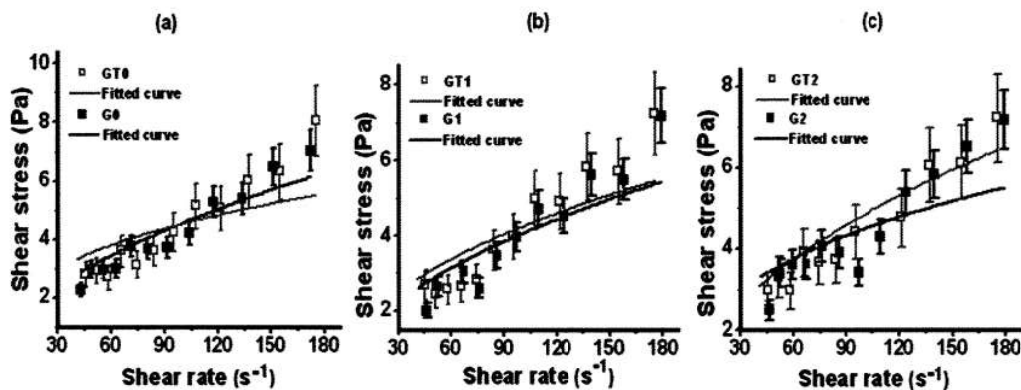


Fig.20. Shear stress vs. shear rate for different FFs: (a) GT0, (b) GT1, and (c) GT2. For the sake of comparison, the responses due to un-doped nanoparticle based systems (G0, G1, and G2) have been also included in the respective plots.

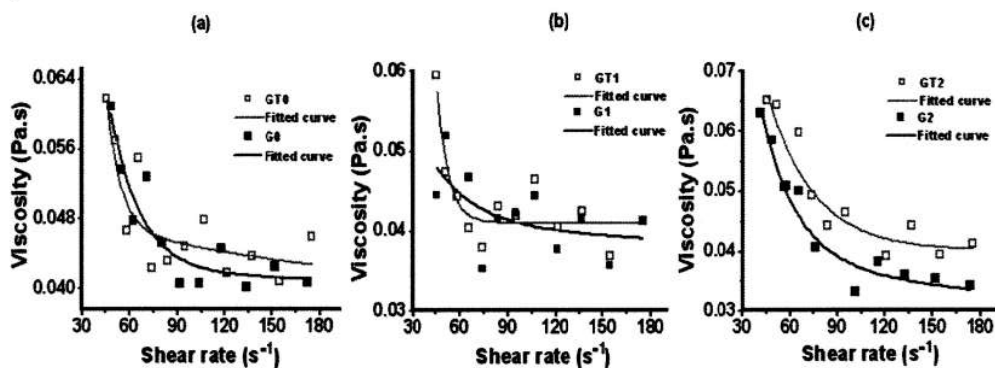


Fig.21. Apparent viscosity vs. shear rate curves for different FFs: (a) GT0, (b) GT1, and (c) GT2. For comparison, the response due to G0, G1, and G2 specimens are also included in the respective plots.

3. Important findings-at a glance

- In magnetite nanoparticle based FFs, γ - irradiation leads to particle size enhancement when subjected to high dose (2.635 kGy), whereas in Gd_2O_3 nanoparticle based FFs, the particle size remained intact for that dose.

- The Faraday rotation (FR) of Fe_3O_4 nanoparticle based FFs increases with increasing applied magnetic field and tend to saturate beyond a critical field. The irradiation effect is manifested as enhanced rotation with γ -dose. In addition, the enhanced FR is ascribed to increased Fe^{2+}/Fe^{3+} charge -transfer capacity and more MNP chain-forming capacity.

M.Devi, R. Das, D.Mohanta, K.K.Baruah and A. Saha, Appl. Phys. A 106: 757-763 (2012). DOI 10.1007/s00339-011-6678-4

-In case of linear dichroism (LD), there exists a noticeable change (about 10% for γ -irradiated Gd_2O_3 nanoparticle based FF than pristine FFs) in the absorbance along the parallel polarization direction as compared to its counterpart. This could be attributed to the collective role of the point defects in field induced one-dimensional chains.

N.Paul, M.Devi, D.Mohanta, and A. Saha, J.Appl.Phys., 111, 044904 (2012). DOI: 10.1063/1.3682765

-Rheological properties of Gd_2O_3 nanoparticle based FFs display shear thinning behavior. Also, the fast and slow components, along with power index value, were assessed for both undoped and Tb^{3+} doped Gd_2O_3 nanoparticle based FFs.

N.Paul, S. Hazarika, A. Saha and D.Mohanta, J. Appl. Phys., 114, 134903 (2013). DOI: 10.1063/1.4823786

4. Conclusion and future directions

We have synthesized surfactant coated Fe_3O_4 based and Gd_2O_3 (undoped and Tb doped) based FFs in different carrier media. The prepared FFs were irradiated with γ -irradiation at five selected doses. We have demonstrated optical, spectroscopic, and rheological characteristics of Tb -doped Gd_2O_3 nanoparticle-based FFs and those irradiated with the energetic γ -rays. The rheological feature of undoped and $Tb:Gd_2O_3$ based FF exhibited pseudoplasticity with a non-Newtonian power law behavior having power indices (s) varying in the range of 0.3–0.5. The effect of Tb^{3+} doping and the role of γ -irradiation were clearly witnessed in the optical and rheological properties of the FFs. Magneto-optic characteristics have exhibited an enhanced FR in the case of use of 632.8 nm laser light, and the effective optical path length was found to be increased with the creation of point defects in Gd_2O_3 nanoparticle system. The LD spectral

response, though gives similar trend for pristine and irradiated (Gd_2O_3 based FF) samples; the absorbance along the parallel direction is suppressed for the later cases.

The size and shape dependent and other rare earth impurity doped (Dy, Eu, Y etc.) Gd_2O_3 nanoparticle systems can be assessed with respect to FR and LD responses of the respective FFs. The effect of cationic, anionic and zwitterionic surfactant can also be considered while fabricating REO nanoparticle based novel FFs.

References

- [1] Y.S. Kang, S. Risbud, J.F. Rabolt, P. Stroeve, *Chem.Mater.* **8**, 2209 (1996)
- [2] X.D. Zhou, W. Huebner, *Appl. Phys. Lett.* **79**, 3512 (2001)
- [3] R.A. Nyquist, C.L. Putzig, and M.A. Leugers (eds.), *The Handbook of Infrared and Raman Spectra of Inorganic Compounds and Organic Salts*, Vol. 1, Academic Press, San Diego, 1996.
- [4] Y.D. Wang, S. Zhang, C.L. Ma, and H.D. Li, *J. Lumin.* **126**, 661–664(1997).
- [5] D.L. Rogow, C.H. Swanson, A.G. Oliver, and S.R.J. Oliver, *Inorg. Chem.* **48**, 1533–1541(2009).
- [6] C. Hu, H. Liu, W. Dong, Y. Zhang, G. Bao, C. Lao, Z.L. Wang, *Adv. Mater.* **19** 470 (2007).
- [7] M. Jayasimhadri, B.V. Ratnam, K. Jang, H.S. Lee, S-S. Yi, J-H. Jeong, *Thin Solid Films.* **518** (2010) 6210.
- [8] K. Zhang, T. Holloway, A. K. Pradhan, Y. Cui, P. Bhattacharya, A. Burger, A. Kar, and A. Patra, *Sci. Adv. Mater.* **4**, 649 (2012).
- [8] H.S. Bennett, E.A. Stern, *Phys. Rev.* **137**, A448 (1965)
- [9] M. Ou, B. Mutelet, M. Martini, R. Bazzi, S. Roux, G. Ledoux, O. Tillement, and P. Perriat, *J. Colloid Interface Sci.* **333**, 684 (2009).
- [10] A. A. Rousan, H. M. El-Ghanem, and N. A. Yusuf, *IEEE Trans. Magn.* **25**(4), 3121 (1989).
- [11] B. R. Jennings, M. Xu, and P. J. Ridler, *Proc. R. Soc. London, Ser. A* **456**, 891 (2000).

FUND UTILIZATION CERTIFICATE

(PROJECTS/SCHEMES)

Name of the Nodal Institution/

Department of Organisation : TEZPUR UNIVERSITY

Name of the Project/Scheme : "Investigation of magnetoviscous and magneto-optic properties of novel ferrofluids".

Tezpur University Ref.No. : DoRD/Phy/DM/2047

UGC Reference No. : 37-367/2009(SR)

Certified that out of Rs 11,41,871/- received from the University Grants Commission during the financial year 2010-13 in favour of Tezpur University under the scheme of support for Major Research Project vide UGC letter NoF.No.37-1/2009(ASS)(SR) , Ref 37-367/2009(SR) and F.No 37-367/2009(SR), a sum of Rs. 8,73,873/- (eight lakhs seventy three thousand eight hundred and seventy three only) has been utilized during the financial year 2010-11 (Rs.88,152/), 2011-12 (Rs.5,59,340/-) and 2012-13(Rs.2,26,381/-); respectively, up to 31.03.2013. The fund has been utilized for the purpose for which it was sanctioned and in accordance with the terms and conditions laid down by the University Grants Commission. The unspent amount of Rs.2,67,998/- has been returned by RTGS.



Principal Investigator

Principal Investigator
Title Investigation -- ferrofluids

Department of Physics
TEZPUR UNIVERSITY

Registrar

Registrar
Tezpur University

For SURAJIT CHAKRABORTY & CO
CHARTERED ACCOUNTANTS

12.04.2013
CA SURAJIT CHAKRABORTY
(Proprietor)

Membership No. 305054

Expenditure statement of UGC project entitled: "Investigation of magneto-viscous and magneto-optic properties of novel ferrofluids".

| Sl. No. | Heads of account | Amount allocated (Rs.) | Expenditure during 2010-11 (Rs.) | Expenditure during 2011-12 (Rs.) | Expenditure during 2012-13 (Rs.) | TOTAL expenditure 2010-2013 (Rs.) | Remarks |
|---------|---|------------------------|----------------------------------|----------------------------------|----------------------------------|-----------------------------------|---|
| 1 | Contingency | 30,000/- | 8,746/- | 3,000/- | | 11,746/- | The additional equipment (Rheometer) could not be purchased because of shortage of fund (owing to hike in dollar-rupee exchange rate) |
| 2 | Chemicals and glassware | 40,000/- | 9,105/- | 15,895/- | | 25,000/- | |
| 3 | Field work and travel | 20,000/- | 1,398/- | 19,978/- | | 21376/- | |
| 4 | Fellowships | 3,38,968/- | 68,903/- | 47,225/- | 1,90,581/- | 3,06,709/- | |
| 5 | Equipment (1 st installment= 4,20,000/- 2 nd installment= 3,00,000/- | 7,20,000/- | --- | 4,73,242/- | | 4,73,242/- | |
| 6 | Overheads charge | 35,800/- | --- | | 35,800/- | 35,800/- | |
| | Total | 11,84,768/- | 88,152/- | 5,59,340/- | 2,26,381/- | 8,73,873/- | |

Amount allocated = Rs. 11, 84,768/-

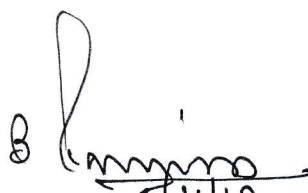
Amount released = Rs. 11, 41, 871/- (1st installment = 6, 44, 800/-, 2nd installment= 4, 97, 071/-)

Amount utilized: Rs. 8, 73, 873/-

Amount refunded: Rs. 2, 67, 998/-


Principal Investigator

Tezpur University


Finance Officer

Tezpur University
Tezpur University


Registrar

Tezpur University
Tezpur University

For SURAJIT CHAKRABORTY & CO.
CHARTERED ACCOUNTANTS


SA SURAJIT CHAKRABORTY
(Proprietor)
Membership No. 305054



विश्वविद्यालय अनुदान आयोग
University Grants Commission
मानव संसाधन विकास मंत्रालय, भारत सरकार
(Ministry of Human Resource Development, Govt. of
India)
बहादुरशाह जफर मार्ग नई दिल्ली -110002
Bahadurshah Zafar Marg, New Delhi-110002



F.No. 37-367/2009 (SR)
The Registrar,
Tezpur University
Napam-784027, Assam.

January 2018

L 6 FEB 2018

Sub: - Major Research Project entitled "**Investigation.....ferrofluids**" awarded to
Dr. Dambarudhar Mohanta, Department of Physics.

Sir,/ Madam,


Please refer to your letter no. **Nil** dated **10.02.2015** on the above subject. The amount of **Rs. 2,67,998/- (Unspent balance of Rs. 2,73,012/- (-) Grant due of Rs. 5,014/-)** has been received in UGC account as unspent balance along with interest. In this regard, I am to inform you that the accounts of the above project may be treated as settled.

Yours faithfully,

(Suresh Rani)
Under Secretary

Copy to:-

Dr. Dambarudhar Mohanta,
Department of Physics.
Tezpur University
Napam-784027, Assam.


(Arun Kumar Sinha)
Section Officer